Numerical Investigation of Influence of Reservoir Heterogeneity on Electricity Generation Performance of Enhanced Geothermal System

Yuchao Zeng [1,2], Liansheng Tang [1,2,*], Nengyou Wu [3,4], Jing Song [1,2] and Zhanlun Zhao [1,2]

[1] School of Earth Science and Engineering, Sun Yat-sen University, Guangzhou 510275, China;
    zengyuc@126.com (Y.Z.); songj5@mail.sysu.edu.cn (J.S.); zhaozhlun@mail2.sysu.edu.cn (Z.Z.)

[2] Guangdong Provincial Key Laboratory of Mineral Resources & Geological Processes,
    Guangzhou 510275, China

[3] Laboratory for Marine Mineral Resources, Qingdao National Laboratory for Marine Science and Technology,
    Qingdao 266071, China; wuny@ms.giec.ac.cn

[4] Qingdao Institute of Marine Geology, China Geological Survey, Qingdao 266071, China

* Correspondence: eestls@mail.sysu.edu.cn; Tel.: +86-20-8411-2113

check for
updates

Abstract: The enhanced geothermal system (EGS) reservoir consists of a heterogeneous fracture network and rock matrix, and the heterogeneity of the reservoir has a significant influence on the system's electricity generation performance. In this study, we numerically investigated the influence of reservoir heterogeneity on system production performance based on geological data from the Gonghe Basin geothermal field, and analyzed the main factors affecting production performance. The results show that with the increase of reservoir heterogeneity, the water conduction ability of the reservoir gradually reduces, the water production rate slowly decreases, and this causes the electric power to gradually reduce, the reservoir impedance to gradually increase, the pump power to gradually decrease and the energy efficiency to gradually increase. The fracture spacing, well spacing and injection temperature all have a significant influence on electricity generation performance. Increasing the fracture spacing will significantly reduce electric power, while having only a very slight effect on reservoir impedance and pump power, thus significantly decreasing energy efficiency. Increasing the well spacing will significantly increase the electric power, while having only a very slight effect on the reservoir impedance and pump power, thus significantly increasing energy efficiency. Increasing the injection temperature will obviously reduce the electric power, decrease the reservoir impedance and pump power, and thus reduce energy efficiency.

Keywords: reservoir heterogeneity; enhanced geothermal system; electricity generation; performance; influence

1. Introduction

1.1. Background

The enhanced geothermal system (EGS) adopts artificial circulating water to extract heat from the fractured hot dry rock (HDR) at a depth of 3–10 km, and is an effective approach to exploiting the high-temperature geothermal energy stored deep in the earth [1]. All over the world, the total EGS resource reserves within a 10km depth amounts to about 40–400 MEJ (1 EJ = 10^{18} J), approximately 100–1000 times the quantity of fossil energy [2]. In China, total EGS resource reserves within a 3–10 km depth amounts to 20.90 MEJ; if the recoverable fraction is taken as 2%, the recoverable EGS resource amounts to 4400 times the total annual energy consumption of China in 2010 [3]. Compared with

other renewable energy sources, the EGS resource is very suitable for generating base-load electric power, with nearly no pollution emissions and with a high utilization efficiency [1]. It is predicted that there will be commercial exploitation of EGS in the next 15 years, with large scale utilization of EGS to generate electricity by 2030 [1]. It is suggested that EGS will provide about 100,000 MW electric power by 2050 in the USA and this will occupy about 10% of total electricity generating capacity [1].

The field tests and experimental studies of EGSs are time-consuming, expensive and very difficult, while numerical studies are very fast, lower cost and easy, thus numerical simulation studies of EGS have received more and more attention all over the world and have made important progress in recent years. Two issues need to be considered in the simulation of EGS reservoirs: fracture representation and simplification of the coupled hydraulic-thermal-mechanical-chemical interaction between the fractured rock and circulating water [4,5]. For fracture representation, there are two main types of method: the equivalent continuum method (ECM) and the discrete fracture network (DFN) method [4,5]. The ECM will regard the actually discrete and interconnected fracture network as continuous porous media and use the mature theories of fluid flow in porous media to describe the water seepage and heat transfer process in the fractured rocks, and this method is mainly used for densely fractured reservoirs [6–10]. The commonly used ECM includes the equivalent porous media (EPM) method, the double-porosity method (DPM) and the multiple interacting continua (MINC) method. The DFN method considers the fracture orientation, spacing and other mechanical properties to establish a fracture network model [4–10]. For simplification of the multiphysics field, recently, the coupling between water flow and heat transfer has been most important and most considered, while the models considering the coupling among the hydraulic, thermal and mechanic effects are increasing [4–10].

The EPM method is mainly used to model densely fractured reservoirs where fracture spacing is small and fracture density is high, especially for average fracture spacing less than 2–3 m [4–10]. Birdsell et al. used the EPM method to develop a three-dimensional model of fluid, heat and tracer transport in the Fenton Hill HDR reservoir [11]. McDermott et al. used the EPM method to analyze the influence of coupled processes on differential reservoir cooling in heat extraction from crystalline rocks [12]. Watanabe et al. used the EPM method to study the uncertainty of thermo-hydro-mechanical coupled processes in heterogeneous porous media [13]. Zeng et al. adopted the EPM method to analyze the electricity generation potential from the EGS reservoirs at Desert Peak geothermal and Yangbajing geothermal field [5,14–19]. Cheng et al. employed the EPM method to analyze the influencing factors of heat extraction from EGSs considering water losses [20]. Based on the EPM method, Hu et al. established a novel fully-coupled flow and geomechanics model in EGS reservoirs [21].

When the average fracture spacing is higher than 10 m, we must consider the temperature difference between rock and water, and the DPM or MINC method is more reasonable for this [4,5]. Sanyal et al. employed the DPM method to analyze the power generation prospects of EGS at the Desert Peak geothermal field [22]. Taron et al. used the DPM method to study the hydrologic-thermal-mechanical-chemical processes in the EGS reservoir [23,24]. Gelet et al. adopted the DPM method to establish a hydro-thermo-mechanical coupled model in local thermal non-equilibrium for fractured HDR reservoirs and found that fluid loss is high initially and decreases over time [25,26]. Benato et al. used the DPM simulator TFReact to analyze the mechanisms influencing permeability evolution during the reservoir stimulation and circulation at Desert Peak geothermal field [27]. Pruess et al. used the MINC method to evaluate the heat extraction rate from EGS reservoirs where the heat transmission fluid is either CO_2 or water [28,29]. Spycher et al. used the MINC method to establish a phase-partitioning model for CO_2-Brine mixtures at elevated temperatures and pressures and applied it to CO_2-EGSs [30]. Borgia et al. used the MINC method to analyze salt precipitation in the fractures of a CO_2-EGS [31]. Xu et al. used the MINC method to calculate the power generation potential of an EGS by water circulating through two horizontal wells in the Gonghe Basin geothermal field [32]. Zeng et al. employed the MINC method to compute the electricity generation potential at the Yangbajing geothermal field [33].

If the data from reservoir fracture distribution are adequate, the DFN model can be adopted, and the use of the DFN method has been increasing recently [4–10]. Baujard et al. used the DFN model to study the impact of fluid density on the pressure distribution and stimulated volume in the Soultz HDR reservoir and found that the density difference between the in situ reservoir fluid and the injected fluid might play a significant role in the hydraulic stimulation of the reservoir [34]. Kolditz et al. used the DFN model to study fluid flow and heat transfer in fractured crystalline rocks in Rosemanowes HDR reservoir and they also made long-term predictions of the thermal performance of HDR systems [35,36]. Jing et al. adopted the stochastic DFN model to study the heat extraction performance of EGS and found that rock thermoelasticity has an obvious effect on the production temperature [37–39]. Based on the DFN model, Sun et al. studied heat extraction in EGS with the hydraulic-thermal-mechanical coupling method and the results show the significance of taking into account the hydraulic-thermal-mechanical (HTM) coupling effect when investigating the performance and efficiency of EGS [40,41].

Though much important progress has been made in recent years, most fractured reservoirs represented by the ECM are homogeneous and the reservoir heterogeneity is not taken into account [4–10]. In fact, because the formation is usually layered and the hydrofracture effect is commonly heterogeneous, the EGS reservoirs are generally heterogeneous [1]. A report from Huang et al. [42] has indicated that reservoir heterogeneity has a significant influence on the heat production performance of EGS, but they only discussed the quantitative relation between the heat extraction ratio and the reservoir heterogeneity. There are quantitative relationships between the electric power, flow impedance, energy efficiency and the reservoir heterogeneity, however recently there is a lack of deep and systematic studies on these quantitative relations [4–10]. In order to analyze the influence of reservoir heterogeneity on the electricity generation performance of the EGSs, in this work we established the numerical model of the EGSs and discussed the influence of reservoir heterogeneity on electricity generation performance in detail based on the geological data of the Gonghe Basin geothermal field [32]. These will lay a good foundation for future research and development of EGSs at the Gonghe Basin geothermal field.

1.2. Research Objectives

The research objectives of this work are to establish a numerical model of EGS with heterogeneous reservoir and to reveal the influence of reservoir heterogeneity on system electricity generation performance.

The novelty of this work is in the following three features. First, we used the MINC method to represent the fractured reservoir and the temperature difference between circulating water and rock matrix was taken into consideration. Second, the layered EGS reservoir with heterogeneous permeability was considered and the corresponding numerical model was established. Third, through a comparison with a homogenous reservoir we examined the impact mechanism of the reservoir heterogeneity on system production performance.

2. Electricity Generation Method and Well Design

2.1. Heat Production Method

In order to deeply analyze the influence of reservoir heterogeneity on system production performance, in this work we considered a five-spot well configuration at the Gonghe Basin geothermal field to mine the heat—namely four production wells at corners and one injection well in the center, as shown in Figure 1. The distance is 1000 m between two adjacent production wells. Only one quarter of the domain needs to be simulated due to symmetry. This kind of well configuration is usually used to analyze heat mining performance [28–31]. Based on the geological data at Gongbe Basin geothermal field, in this work we aimed to mine the heat at a depth of 2700–3200 m [32]. The vertical wells are perforated over the whole reservoir height of 500 m to obtain maximum water production rate and

thermal power. As shown in Figure 2, along the circumference of the vertical wells there are 8 grooves evenly distributed and previous studies have shown that this kind of well design can obtain a much higher mining efficiency [14–19]. The whole injection rate or production rate is distributed across the four gridblocks where the well is located, thus one gridblock will only represent the production rate through two grooves, namely one quarter of the whole production rate [14]. We used the constant water production rate method to mine the heat in the fractured rocks. For the production well, we installed a downhole pump to maintain the bottomhole production pressure P_{pro} at a constant; for the injection well, we installed an injection pump to maintain the injection rate q at a constant. Field tests and numerical simulations all show that this kind of injection and production method can greatly reduce reservoir impedance and water losses [4,5]. When injecting cold water into the fractured reservoir, the formation pressure will rise. To avoid second reservoir growth and water losses, P_{inj} must be lower than the minimum reservoir principal stress [5]. Based on the experience from the oil and gas industry, in order to avoid the second fracture growth P_{inj} must be kept below an upper limit P_{max} [5]:

$$P_{inj} < P_{max} \tag{1}$$

where $P_{max} = fP_{W0}$; P_{W0} is the initial pressure of the wellbore; $f = 1.2$ is the safety factor and is determined by the actual geologic conditions [5]. At the Gonghe Basin geothermal field, the initial wellbore pressure of the injection well at the intermediate depth of 2950 m is $P_{W0} = 29.20$ MPa, so the $P_{max} = 35.04$ MPa in this work. The initial wellbore pressure of the production well at the intermediate depth of 2950 m is 29.20 MPa. Based on the engineering data at Desert Peak geothermal field, under current pump technology the maximum pressure drawdown in the bottomhole production well is 3.40 MPa [5]. Therefore, in this work the minimum bottomhole production pressure P_0 at the production well is (29.20 − 3.40) = 25.80 MPa, and the production pressure P_{pro} is decreased to 25.80 MPa to maintain continuous production.
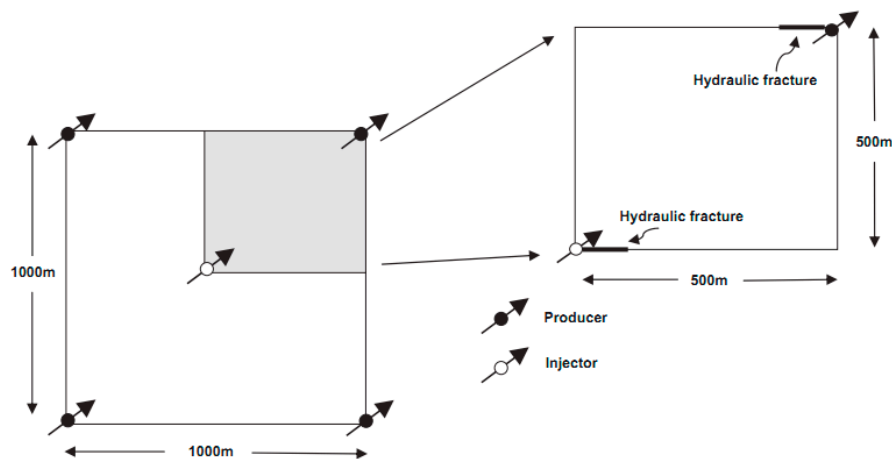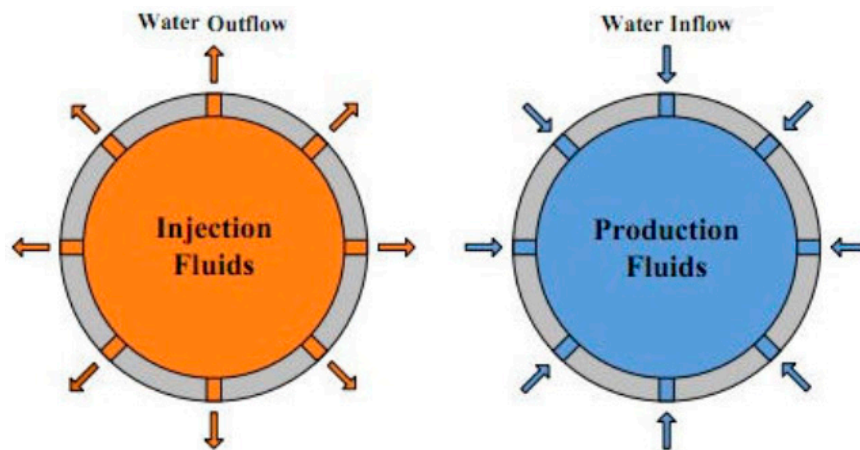

Figure 1. Five-spot well pattern for the 2700–3200 m fractured reservoir.

Figure 2. Well design used in the five-spot enhanced geothermal system (EGS) at the Gonghe Basin geothermal field.

2.2. Electricity Generation Method

So far, the commonly used methods for electricity generation in the geothermal industry include the dry steam system, the flash system and the binary system, and the applicable conditions and efficiency of each system are all different [1]. The dry steam system is mainly used for high-temperature geothermal resources where the geothermal fluid is mainly in the form of steam. The flash system and binary system are mainly used for medium and low temperature geothermal resources where the geothermal fluid is mainly in the form of hot liquid. The factors affecting the conversion efficiency of the geothermal power plant includes production temperature, system design, heat loss from equipment, non condensable gases (NCG) content, turbines and generator efficiency and other factors [43]. At the Gonghe Basin geothermal field, the average temperature of the fractured formation at a depth of 2700–3200 m is about 180 °C, the most suitable method is the binary system according to reports from Xu et al., so in this numerical study we used the binary system to calculate the production performance [32].

The scheme of the basic binary geothermal power plant at Gonghe Basin geothermal field was reported by Xu et al. in Reference [32]. Based on the studies from Zeng et al., the optimized injection temperature for the circulation system is 60 °C [5]. Neglecting the temperature drop when the water flows from the production well to the power plant, the production temperature T_{pro} is regarded as the inlet temperature for the power plant. The mean annual temperature in the Gonghe Basin is 4.1 °C [32], thus the heat rejection temperature of $T_0 = 277.25$ K is used for electric power calculation. Based on the second law of thermodynamics, the fraction of the total produced heat that can be converted to the maximum mechanical work f_R can be calculated as Equation (2), in which the T_0 and T_{pro} are all absolute temperature.

$$f_R = 1 - \frac{T_0}{T_{pro}} \tag{2}$$

3. Numerical Method

3.1. Mathematical Model

Because the pressure in the fractured reservoir is great enough, the water remains in the liquid state when temperature is at 180 °C, thus it is water saturated single liquid flow in the fractured formation. The mass conversation equation is (3), where ρ is water density, ϕ reservoir porosity, V the velocity vector.

$$\frac{\partial(\rho\phi)}{\partial t} + \nabla\cdot(\rho V) = 0 \tag{3}$$

The momentum conservation equation for single liquid flow is the classical Darcy's law, as Equations (4)–(6), where V_x, V_y and V_z is velocity component along the x, y and z direction, K_x, K_y and K_z is reservoir permeability along the x, y and z direction, μ the dynamic viscosity, P the pressure, $g = 9.80$ m/s^2 the acceleration of gravity.

$$V_x = -\frac{K_x}{\mu}\frac{\partial p}{\partial x} \tag{4}$$

$$V_y = -\frac{K_y}{\mu}\frac{\partial p}{\partial y} \tag{5}$$

$$V_z = -\frac{K_z}{\mu}\left(\frac{\partial p}{\partial y} + \rho g\right) \tag{6}$$

Assuming that the rock matrix and circulating water is in local thermodynamic equilibrium, namely the rock temperature is equal to the water temperature, in the rock the heat transfer is conduction, and in the water the heat transfer is convection and conduction, thus the energy conservation equation for single liquid flow is Equation (7):

$$[\phi(\rho c_p)_f + (1-\phi)(\rho c_p)_s]\frac{\partial T}{\partial t} + (\rho c_p)_f (V \cdot \nabla)T = [\phi k_f + (1-\phi)k_s]\nabla^2 T \tag{7}$$

where T is the temperature, $(\rho c_p)_f$ is product of water density and water specific heat capacity, $(\rho c_p)_s$ is product of solid density and solid specific heat capacity. c_p is specific heat capacity, k_f is water heat conductivity, and the k_s is solid heat conductivity. Because in this work the variation of reservoir pressure and temperature is very great and its influence on water density and viscosity is significant, we considered that the water density and viscosity are functions of pressure and temperature, as Equations (8) and (9). In this paper, the ρ and the μ are calculated from steam table equations as given by the International Formulation Committee [44]. For more information about the state equations, the reader can refer to Reference [44].

$$\rho = \rho(p, T) \tag{8}$$

$$\mu = \mu(p, T) \tag{9}$$

3.2. The MINC Method

For EGS reservoirs with large fracture spacing, the MINC method is an effective approach for modeling fluid flow and heat transfer. In the fractured reservoirs, matrix blocks with low permeability are embedded in the fracture network, and fluid flow mainly occurs through the fractures [44]. For describing the fluid and heat transport process in the fractured media, it is necessary to resolve the driving temperature, pressure and mass fraction gradients at the matrix/fracture interface. In the MINC approach, the pressure and temperature changes in the matrix are controlled locally by the distance from the fractures. Based on Xu et al. [32], in this work the matrix blocks are divided into four subgrids with volume fractions of 0.08, 0.2, 0.35 and 0.35. The fracture domain occupies a volume fraction of 0.02. In this work, the TOUGH2-EOS1 codes are employed to carry out the simulation. For more information about the MINC method and the TOUGH2 codes, the reader can refer to Reference [44].

3.3. Domain, Grid and Parameters

As stated above, in this work we mainly aim to exploit the heat stored in the fractured reservoir at a depth of 2700–3200 m and the distance between two adjacent production wells is 1000 m, as shown in Figure 1. Because of symmetry, only one quarter of the whole domain needs to be simulated, thus the actual calculated domain is 500 m × 500 m × 500 m. As shown in Figure 3, in the horizontal direction the grid that is within 50 m of the wells is refined, the width of every gridblock is 5 m and there are

10 gridblocks near the wells. For the other subdomain that is not near the wells, the 400 m length is evenly divided into 8 gridblocks, and the width of every gridblock is 50 m. Therefore, there are a total of 28 gridblocks in the x direction and the y direction. In the vertical direction, the 500 m height is evenly divided into 10 gridblocks, and the height of every gridblock is 50 m. With this grid arrangement, in the simulated domain there are total $28 \times 28 \times 10 = 7840$ gridblocks. Based on Section 3.2, the reservoir domain is further divided into 5 continua for the MINC method, thus there are total $7840 \times 5 = 39,200$ gridblocks for the whole calculated domain. Under reference condition, we assumed that after hydrofracture, the fracture spacing is 50 m [32]. According to Pruess et al. [29], the conductive heat transfer between the impermeable cap rock or base rock and the permeable reservoir can be neglected for the fracture spacing of 50 m, thus in this work the conductive heat transfer between the confined rocks and the reservoir is neglected and only the heat transfer process within the reservoir is considered in this simulation. Assuming the surrounding rocks are impermeable, the water loss can be neglected [5], and the water injection rate q_{inj} is equal to the water production rate q_{pro}:$q_{inj} = q_{pro}$. Neglecting the water loss can greatly simplify the calculation of reservoir performance, and this has been adopted from previous studies by Zeng et al. and Xu et al. [4,5,32].

In order to investigate the influence of reservoir heterogeneity on system electricity generation performance, under reference conditions we considered three permeability distribution patterns, as shown in Figure 4. In this work, we assumed that the permeability is independent of the porosity, namely the relationship between permeability and porosity is not taken into account. There are 10 layers in the vertical direction, and the average permeability of the 10 layers is maintained at 50 mD ($1\ mD = 1.0 \times 10^{-15}\ m^2$). For the first case R1, we considered a homogenous reservoir of uniform permeability, and the permeability of every layer is 50 mD. For the second case R2, we considered a heterogeneous reservoir, in which the permeability of the 5th and 6th layer is 200 mD, and the permeability of the remaining 8 layers is 12.50 mD. For the third case R3, we considered a heterogeneous reservoir, in which the permeability of 3rd layer, 4th layer, 7th layer and 8th layer is 100 mD, and the permeability of the remaining 6 layers is 16.67 mD. We can easily find that the R1 reservoir is homogenous, the R2 reservoir is most heterogeneous, and the heterogeneity of the R3 reservoir is in between. Namely, the ranking for the heterogeneity of the three cases is: R2 > R3 > R1. Based on the studies from Xu et al. at the Gonghe Basin geothermal field, the fracture porosity is taken as 0.5 [32]. The other model parameters are listed in Table 1, in which most are referred to work of Xu et al. [32].
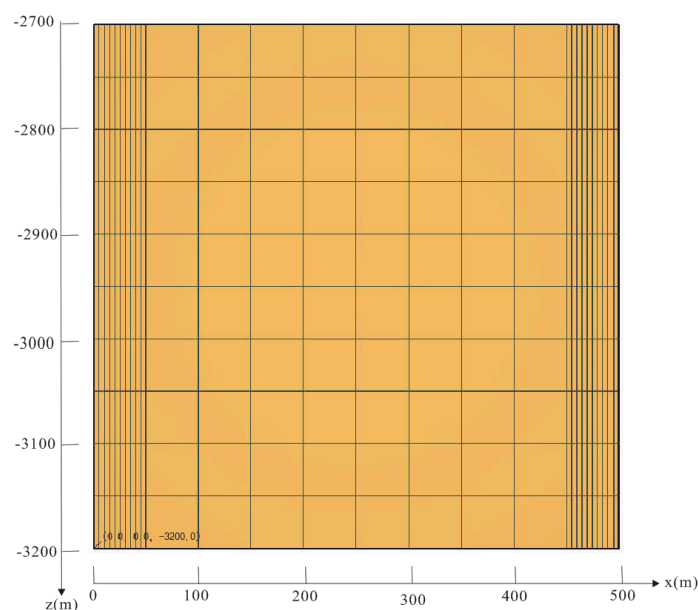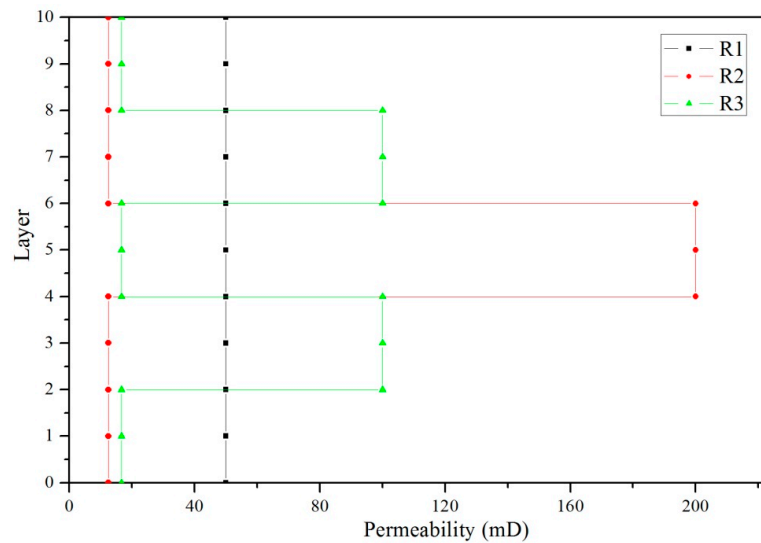

Figure 3. Simulation domain and grid used in this work.

Figure 4. The permeability distribution pattern for the three cases: R1, R2 and R3.

Table 1. EGS reservoir properties and conditions at the Gonghe Basin geothermal field [32].

Parameter	Value
Rock grain density	2650 kg/m^3
Rock specific heat	1000 J/(kg·K)
Rock heat conductivity	2.50 W/(m·K)
Fracture system volume fraction	2%
Fracture spacing	50 m
Porosity in fracture system	0.5
Porosity in matrix	1.0×10^{-5}
Permeability in matrix	1.0×10^{-18} m^2
Injection temperature	60 °C (275.571 kJ/kg)
Bottomhole production pressure	25.80 MPa
Productivity index	5.0×10^{-12} m^3

3.4. Boundary and Initial Conditions

Neglecting the conductive heat transfer between the cap rock or base rock and the reservoir and assuming that the surrounding rocks are impermeable, the topmost and bottommost boundaries in Figure 3 are all no-flow for mass and heat. Because of symmetry, the lateral boundaries in Figure 3 are also all no-flow for mass and heat. The initial pressure is $P = -0.0088z + 3.24 (\text{MPa})$, and the initial temperature is 180 °C [32].

4. Influence of Reservoir Heterogeneity on the Electricity Generation Performance

4.1. The Determination of Water Production Rate

In previous studies, we have clearly stated the determination method for the water production rate [4]. A lower water production rate will decrease electric power and reduce the practical application value of the system. With an increase of the water production rate, the injection pressure gradually increases; however, for given reservoir conditions, the tolerable maximum injection pressure is finite. Based on (1), we gradually increased the water production rate and calculated the corresponding injection pressure under various conditions. With the increase of water production rate, the production temperature T_{pro} rapidly declines [4,5]. For engineering applications, during the exploiting period the drop of the production temperature T_{pro} should be less than 10%, or the decline of reservoir temperature will be too great, and this will affect the regenerability of the geothermal resource [4,5]. As stated above, based on the two principles that the maximum injection pressure must be lower than

P_{max} = 35.04 MPa and the production temperature drop must be less than 10%, we can determine the available maximum water production rate, and under this water production rate the system can obtain maximum electric power. Because of symmetry the total water production rate and thermal power of the five well system is 4 times that of the simulated domain. Figure 5 shows the change of the injection pressure P_{inj} corresponding to the three reference cases and Figure 6 shows the change of the production temperature T_{pro} corresponding to the three reference cases. For the R1 reservoir, the water production rate for the simulated domain is 40 kg/s, thus the total water production rate of the five well system is 160 kg/s. For the R2 reservoir, the water production rate for the simulated domain is 17.50 kg/s, thus total water production rate of the five well system is 70 kg/s. For the R3 reservoir, the water production rate for the simulated domain is 30 kg/s, thus total water production rate of the five well system is 120 kg/s. It can be easily found that with the increase of the reservoir heterogeneity, namely R1 < R3 < R2, the corresponding water production rate gradually decreases. Though the average permeabilities of the three reference cases are the same, for the heterogeneous reservoir, the permeabilities of the various layers are different and with the increase of the reservoir heterogeneity, the fluid conduction ability of the reservoir is decreasing, thus the available water production rate gradually declines. It can be seen in Figure 5 that with the increase of the reservoir heterogeneity—namely R1 < R3 < R2—the corresponding injection pressure gradually decreases. As stated above, the injection pressure is mainly determined by the water production rate and a higher water production rate means a higher injection pressure. Because with the increase of reservoir heterogeneity—namely R1 < R3 < R2—the water production rate gradually decreases, thus the corresponding injection pressure gradually declines. It can also be seen in Figure 5 that during the period that the injection pressure is gradually increasing, the maximum injection pressure under the three reference cases are all lower than P_{max} = 35.04 MPa. This is mainly due to the decline of the reservoir temperature, causing an increase of the water viscosity and the rise of reservoir impedance [4,5]. This is in agreement with previous studies by Zeng et al. [4,5]. Figure 6 shows that changes in the production temperature under three cases are consistent for the determined water production rate, and the production temperature decreases to about 162 °C, a reduction of about 10%. This indicates that the reservoir heterogeneity has only a very slight influence on the production temperature for the determined water production rate. Though reservoir heterogeneity increases local ability to conduct water, it decreases the global ability to conduct water and heat, thus it has only a very slight influence on the production temperature when reducing the water production rate.
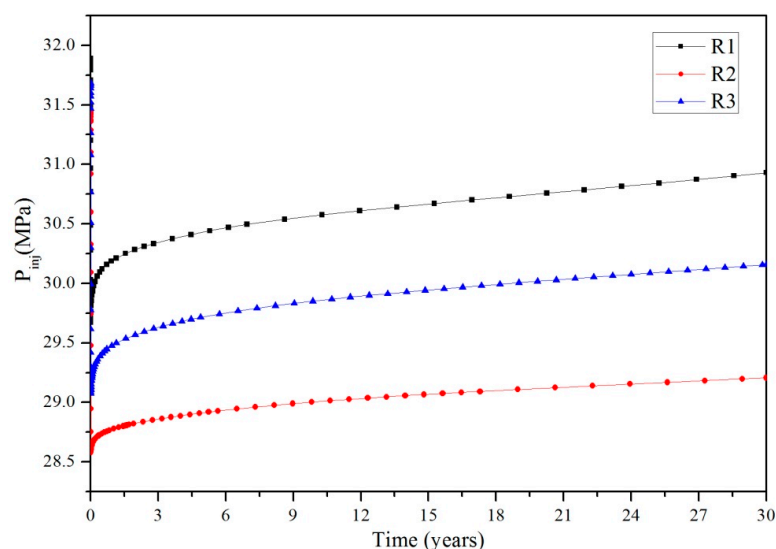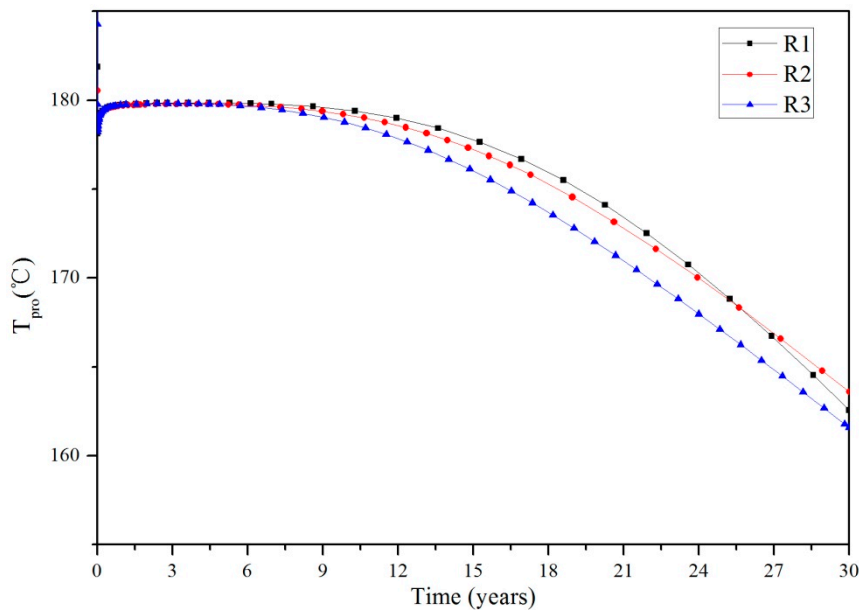

Figure 5. Change of the injection pressure P_{inj} corresponding to the three reference cases.

Figure 6. Change of the production temperature T_{pro} corresponding to the three reference cases.

4.2. Influence of Reservoir Heterogeneity on the Electric Power

For the binary system, if the water production rate of the simulated domain is q, the total water production rate for the five well system is Q = 4q. In a more realistic environment, it is very likely that there will be a short circuit between the injection well and one of the production wells; therefore, that production well will produce more than the rest. For simplification, in this work we have assumed there is no short circuit between the injection well and production wells, and that the water production rate of each production well is equal. If the injection specific enthalpy of the injection water is h_{inj}, the production specific enthalpy is h_{pro}, then the thermal power of the system W_h can be calculated by Equation (10), where the temperature drop, when flowing from production well to power plant, is neglected [5]. The h_{pro} is calculated according to the bottomhole production temperature and pressure: $h_{pro} = h_{pro}(P_{pro}, T_{pro})$. As stated above, h_{inj} = 275.571 kJ/kg and is corresponding to T_{inj} = 60 °C.

$$W_h = Q(h_{pro} - h_{inj}) = 4q(h_{pro} - h_{inj}) \tag{10}$$

Based on Equation (2), the fraction of the total produced heat that can be converted to the maximum mechanical work is f_R. If the utilization efficiency of the maximum mechanical work transferred to electric power is 0.45 [4,5], the electric power W_e of the EGS power plant can be calculated as Equation (11). As stated above, at the Gonghe Basin geothermal field, T_0 = 277.25 K.

$$W_e = 0.45 f_R W_h = 0.45 Q(h_{pro} - h_{inj})(1 - \frac{T_o}{T_{pro}}) = 1.8q(h_{pro} - h_{inj})(1 - \frac{T_o}{T_{pro}}) \tag{11}$$

Figure 7 shows the change in electric power over 30 years under three reference cases. Based on previous studies, the change of the electric power of the EGS power plant can be divided into two stages: a stable stage and a declining stage [4,5]. During the stable stage, T_{pro} maintains an initial reservoir temperature and the corresponding electric power is also maintained unchanged; during the declining stage, the T_{pro} gradually declines and the corresponding electric power also gradually reduces based on Equation (11). It can be easily seen in Figure 7 that for the R1 reservoir, the electric power W_e is highest, and over the 30 years, the W_e gradually decreases from 13.97 MW to 11.20 MW. For the R3 reservoir, the W_e is in between, and it gradually decreases from 10.45 MW to 8.29 MW. For the R2 reservoir, the W_e is lowest, and it slowly reduces from 6.10 MW to 4.97 MW during the 30 years. According to Figure 6, the T_{pro} are very close in the three reference cases, thus the main

factor affecting the W_e is the water production rate q based on Equation (11). For the R1, R3 and R2 reservoir, the q is 40 kg/s, 30 kg/s and 17.50 kg/s, respectively. The q gradually decreases, thus the corresponding W_e also reduces. This indicates that with the increase of the reservoir heterogeneity, namely R1 < R3 < R2, the water conduction ability of the reservoirs decreases, the corresponding water production rate reduces and the electric power declines. It is clear that during the reservoir stimulation stage, we should control the reservoir to be uniformly stimulated and make the permeability of every layer the same and this will greatly improve the water conduction ability of the reservoir and increase the electric power.
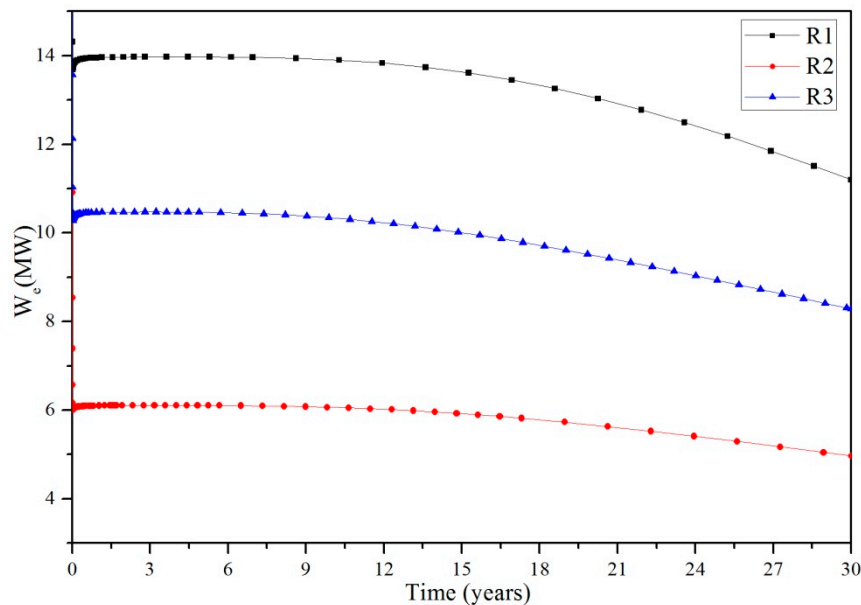
Figure 7. Change of the electric power during the 30 years under the three reference cases.

4.3. Influence of Reservoir Heterogeneity on the Reservoir Impedance

The water flow impedance of the system can be calculated as Equation (12), where P_{pro} = 25.80 MPa. In previous studies, Zeng et al. has analyzed the main factors influencing the flow impedance [4,5], and found that with heat mining the reservoir temperature gradually declines, the water viscosity slowly increases, and this causes the gradual increase of the reservoir impedance.

$$I_R = \frac{P_{inj} - P_{pro}}{q} \tag{12}$$

Figure 8 shows the change of the reservoir impedance over the 30 years under the three reference cases. For the R1 reservoir, over the 30 years the reservoir impedance is lowest, and it gradually increases from 0.097 MPa/(kg/s) to 0.128 MPa/(kg/s). For the R3 reservoir, the reservoir is in between, and it slowly increases from 0.110 MPa/(kg/s) to 0.145 MPa/(kg/s) over the 30 years. For the R2 reservoir, the reservoir impedance is highest, and it increases from 0.160 MPa/(kg/s) to 0.195 MPa/(kg/s) over the 30 years. These indicate that with the increase of the reservoir heterogeneity, namely R1 < R3 < R2, the reservoir impedance increases. As stated above, this is mainly because the reservoir heterogeneity significantly reduces the global water conduction ability of the reservoir; when the average permeability of the various layers is constant, the water conduction ability of the reservoir decreases with the increase of the reservoir heterogeneity, thus the reservoir impedance increases with an increase in the reservoir heterogeneity. In this work, the rock deformation due to mechanics and thermoelasticity is not taken into consideration in the simulation. However, in factual EGS reservoir, as the reservoir cools, the fractures may dilate, and this increases permeability and reduces inter-well impedance.
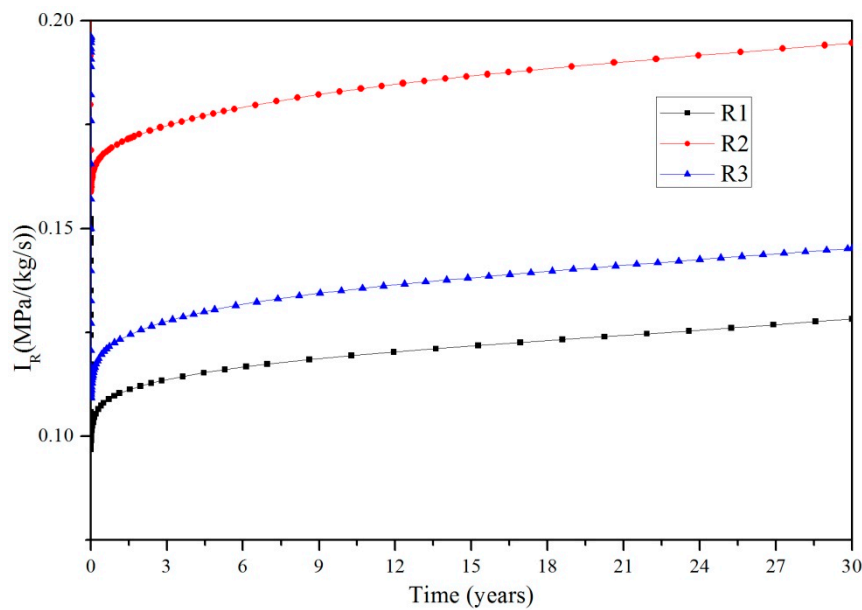
Figure 8. Change of the reservoir impedance during the 30 years under the three reference cases.

4.4. Influence of Reservoir Heterogeneity on the Pump Power

The internal energy consumption $W_p = W_{p1} + W_{p2}$, includes mainly the energy consumed by the injection pump W_{p1} and the production pumps W_{p2} [4,5]:

$$W_{p1} = \frac{4q(P_{inj} - \rho g h_1)}{\rho \eta_p} \tag{13}$$

$$W_{p2} = \frac{4q(\rho g h_2 - P_{pro})}{\rho \eta_p} \tag{14}$$

where h_1 is the depth of the injection well, h_2 is the depth of production well, and η_p = 80% is the pump efficiency [4,5]. Based on these the internal energy consumption W_p is Equation (15):

$$W_p = W_{p1} + W_{p2} = \frac{4q(P_{inj} - P_{pro}) - 4\rho q g(h_1 - h_2)}{\rho \eta_p} \tag{15}$$

In this work, $h_1 = h_2$ = 3200 m, thus the Equation (15) of W_p can be reduced into Equation (16):

$$W_p = W_{p1} + W_{p2} = \frac{4q(P_{inj} - P_{pro})}{\rho \eta_p} \tag{16}$$

In Equation (16), the water density ρ is determined by the reservoir pressure and temperature. When the pressure is within 25.80–31.00 MPa and the temperature is within 60–180 °C, the maximum value of the water density is 996.25 kg/m^3, the minimum value of the water density is 902.61 kg/m^3, thus the average value of the water density is ρ = 949.43 kg/m^3. Based on previous studies from Zeng et al. [4,5], adopting the average value of the water density in Equation (16) is accurate and reliable, thus in this work we used the average density of ρ = 949.43 kg/m^3 for calculation and analysis. Figure 9 shows the change of the pump power W_p during the 30 years under the three reference cases. Based on Equation (16), during the mining period the P_{inj} is increasing, thus the W_p is also gradually rising, and this is in accordance with Figure 9. For the R1 reservoir, the W_p is highest and it gradually increases from 0.82 MW to 1.08 MW. For the R3 reservoir, the W_p is in between and it gradually increases from 0.52 MW to 0.69 MW. For the R2 reservoir, the W_p is lowest and it gradually rises from 0.26 MW to 0.31 MW. So, we can see that with an increase of reservoir heterogeneity—namely R1 < R3

< R2—the W_p gradually decreases. Based on Equation (16), this is mainly because, with the increase of reservoir heterogeneity, the available water production rate declines. Therefore, the water conduction ability reduction caused by the increase of the reservoir heterogeneity can significantly influence the pump power.
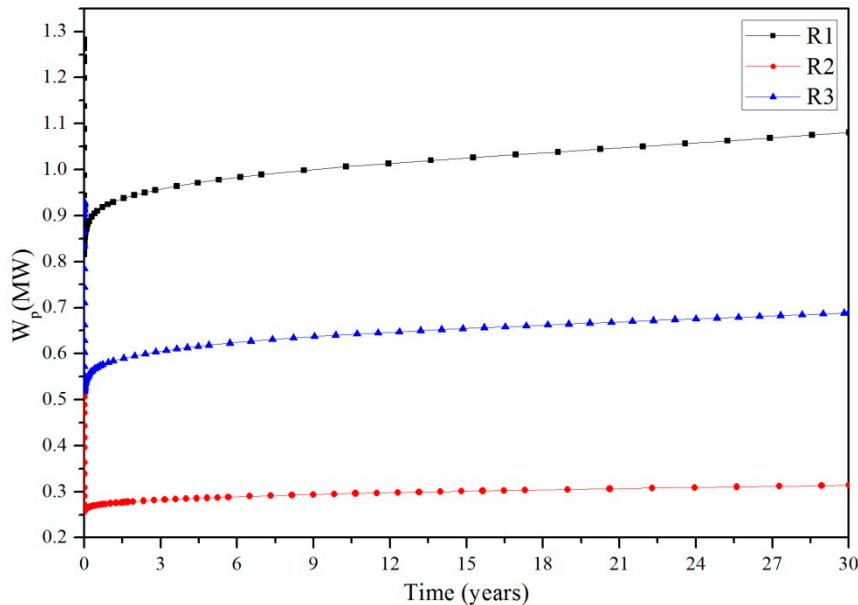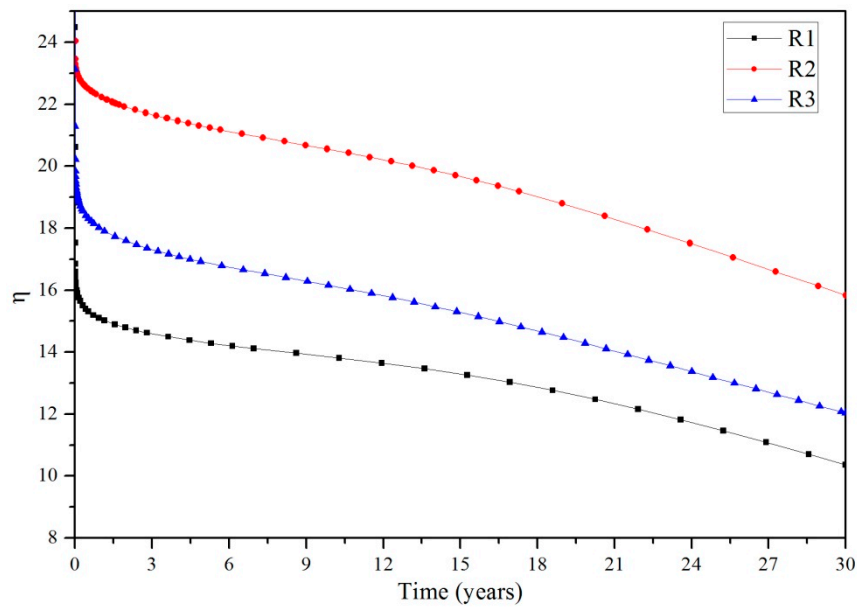

Figure 9. Change of the pump power during the 30 years under the three reference cases.

4.5. Influence of Reservoir Heterogeneity on the Energy Efficiency

The energy efficiency η of the system is defined as the ratio of the total produced electric energy to the internal energy consumption, and can be calculated as Equation (17):

$$\eta = \frac{W_e}{W_P} = \frac{0.45\rho\eta_p(h_{pro} - h_{inj})(1 - T_o/T_{pro})}{(P_{inj} - P_{pro}) - \rho g(h_1 - h_2)} \tag{17}$$

In the calculation of Equation (17), the water density is still taken as the average value of ρ = 949.43 kg/m^3. Figure 10 shows the change of the energy efficiency during the 30 years under the three reference cases. Based on Equation (17), during the heat mining because the T_{pro} and h_{pro} gradually decreases while the P_{inj} gradually increases, the energy efficiency η gradually reduces, and this is in agreement with Figure 10. For the R1 reservoir, the η is lowest and it decreases from 20.62 to 10.36. For the R3 reservoir, the η is in between and it reduces from 23.13 to 12.04. For the R2 reservoir, the η is highest and it decreases from 24.05 to 15.83. So, it can be found that with the increase of the reservoir heterogeneity—namely R1 < R3 < R2—the η rises. Though the reservoir heterogeneity significantly reduces the water conduction ability of the reservoir, under a lower water production rate the system obtains a higher energy efficiency. These are in accordance with previous studies from Zeng et al. [4,5]. Though the heterogeneous reservoir can obtain higher energy efficiency, it decreases the water production rate and also electric power is reduced, thus the economic benefit of the heterogeneous reservoir is still lower than that of the homogenous reservoir.
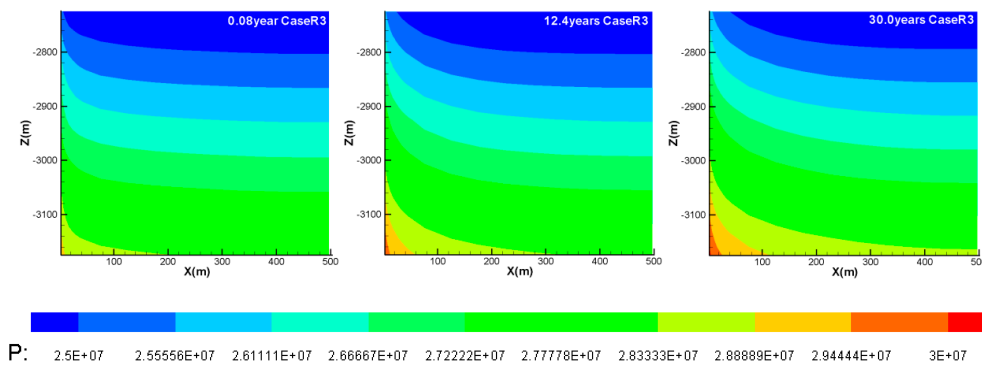
Figure 10. Change of the energy efficiency during the 30 years under the three reference cases.

4.6. Influence of Reservoir Heterogeneity on the Pressure Field

Figure 11 shows the evolution of the spatial distribution of the fracture pressure over the 30 years under the three reference cases. High pressure annular regions gradually form near the injection well, and the fracture pressure declines from the injection well to the production well. With heat mining, the high pressure regions gradually expand, the reservoir pressure gradually increases, and this represents the thermal energy in the reservoir is being gradually extracted out. These are in accordance with previous studies from Zeng et al. [16]. From the comparison among the three reference cases, the distribution and evolution of the fracture pressure are basically identical and this shows that the reservoir heterogeneity has only a very slight influence on the pressure field.
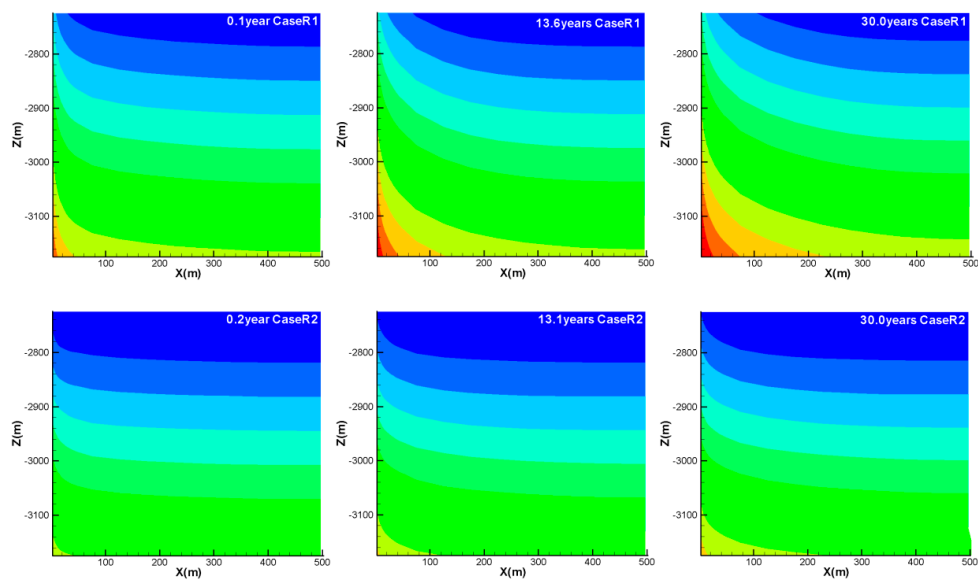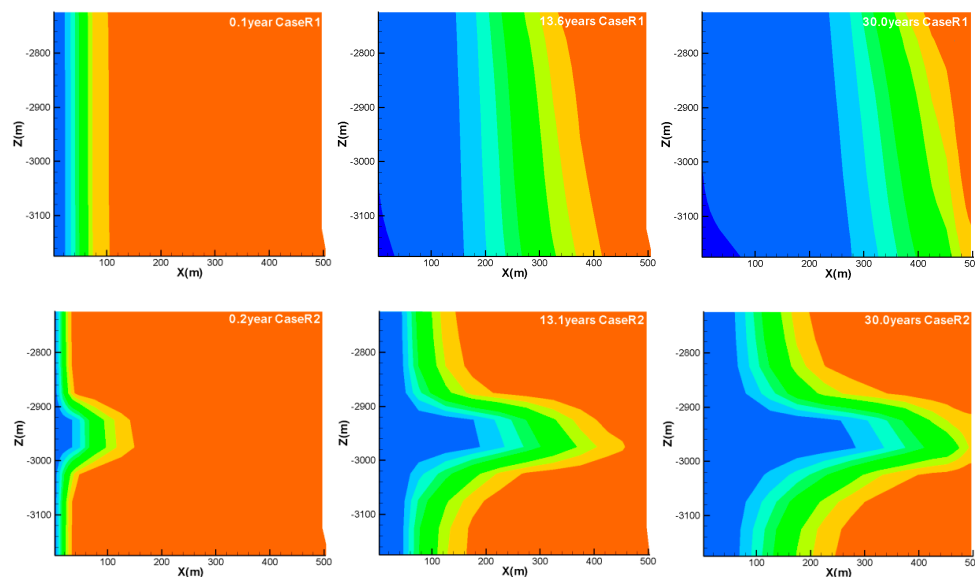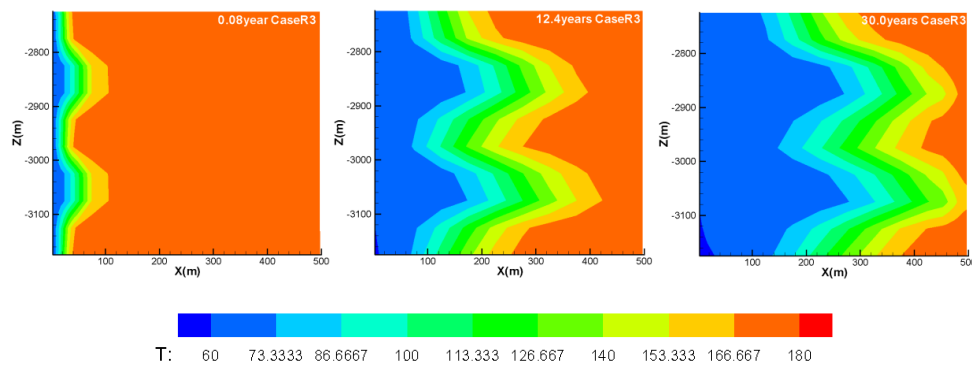

Figure 11. *Cont.*

Figure 11. Evolution of spatial distribution of the fracture pressure (Pa) during the 30 years under the three reference cases.

4.7. Influence of Reservoir Heterogeneity on the Temperature Field

Figure 12 shows the evolution of the spatial distribution of the fracture temperature during the 30 years under the three reference cases. Annular low temperature regions gradually form near the injection well and the fracture temperature gradually increases from the injection well to the production well. With heat mining, the low temperature regions gradually expand, the reservoir temperature gradually declines, and this represents the result of the thermal energy in the reservoir being gradually extracted out. These are in accordance with previous studies from Zeng et al. [16]. Comparing the three reference cases, we find that a cold front forms in the high permeability layer of the heterogeneous reservoir. For the R1 reservoir, the temperature distribution of all the layers are basically identical and a cold front does not develop in which the temperature field is uneven. For the R2 reservoir, there forms one cold front in the two high permeability layers, because in these layers the water seepage velocity is much higher than that in the lower permeability layers. For the R3 reservoir, there forms two cold fronts in the four high permeability layers of the reservoir, also because the water velocity in these layers is much higher than that in the rest layers. These indicate that the reservoir heterogeneity has a significant influence on the fracture temperature field. In higher permeability layers, the water seepage velocity is increased, and there will form cold front, which means the temperature distribution along depth is uneven. The figure also shows that the system can benefit from buoyancy drive due to the temperature difference in the production and injection wells, and these are in agreement with studies from Huang et al. [42].
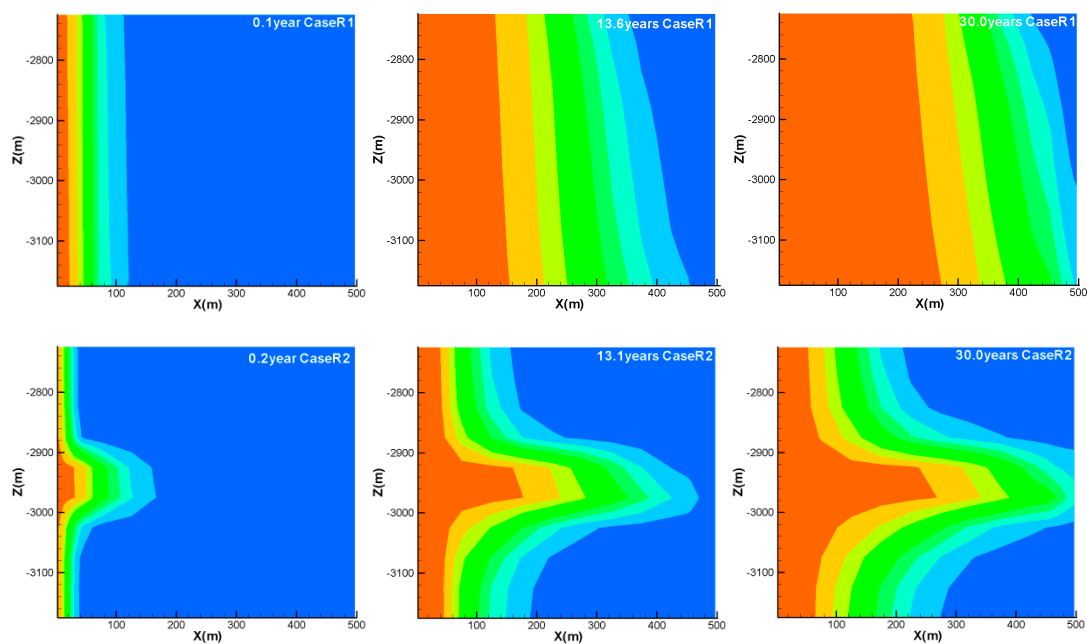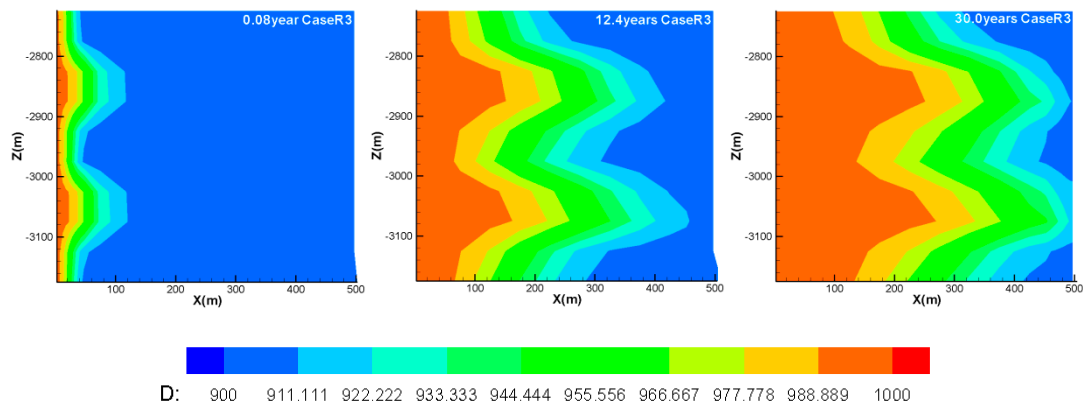

Figure 12. *Cont.*

Figure 12. Evolution of the spatial distribution of the fracture temperature (°C) during the 30 years under the three reference cases.

4.8. Influence of Reservoir Heterogeneity on the Water Density Field

Figure 13 shows the evolution of the spatial distribution of the fracture water density over the 30 years under the three reference cases. Because near the injection well, it is high pressure and low temperature, annular high water density regions form. The water density reduces from the injection well to the production well. With heat mining, the high density regions expand toward the production well, the water density in the reservoir gradually increases, and this represents the result of the thermal energy being gradually extracted from the reservoir. Comparing the three reference cases we can find that in the high permeability layers there forms low density front, while in the low permeability layers the density distribution are basically even. For the R1 reservoir, the water density in each layer is basically identical, and a low density front does not form. For the R2 reservoir, there forms one low density front in the two high permeability layers. For the R3 reservoir, there forms two low density fronts in the four high permeability layers. As stated above, this is mainly because in the high permeability layers the horizontal velocity is much greater than that in the lower permeability layers, thus the low density contours are fronted in the high permeable layers. These indicate that the reservoir heterogeneity has a significant influence on the water density field. Higher permeability will increase the water conduction ability in the layers and there will form low density front, making the density distribution uneven along depth. This is in agreement with the studies by Huang et al. [42].


Figure 13. *Cont.*

Figure 13. Evolution of the spatial distribution of the facture water density (kg/m^3) during the 30 years under the three reference cases.

5. Sensitivity Analysis

Many factors have significant influence on the production performance of the EGSs and previous studies can be found in References [4,19,20,45]. Most important parameters that can be controlled and adjusted are fracture spacing, well spacing and injection temperature [20,45], thus in this study we mainly investigated the influence of the above three parameters. Based on the above three reference cases, we further investigated the sensitivity of electricity generation to the three key parameters: fracture spacing D, well spacing WS and injection temperature T_{inj}. In detail we researched the performance and efficiency characteristics of the following 3 scenarios: (1) increasing D to D = 75 m; (2) increasing WS to WS = 600 m; (3) increasing T_{inj} to T_{inj} = 80 °C. Figures 14–17 show the sensitivity of electric power, reservoir impedance, pump power and energy efficiency to the above three parameters, respectively.
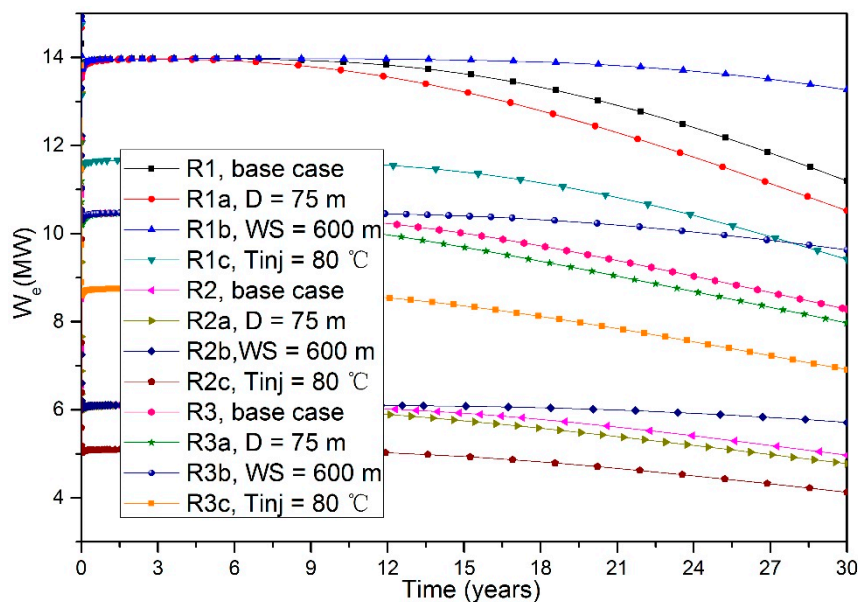
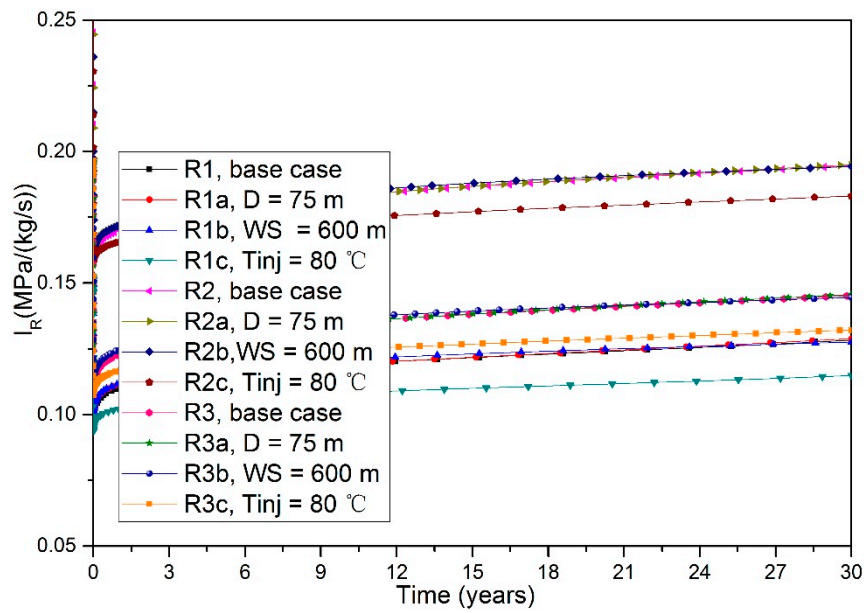**Figure 14.** Sensitivity of electric power to main parameters.

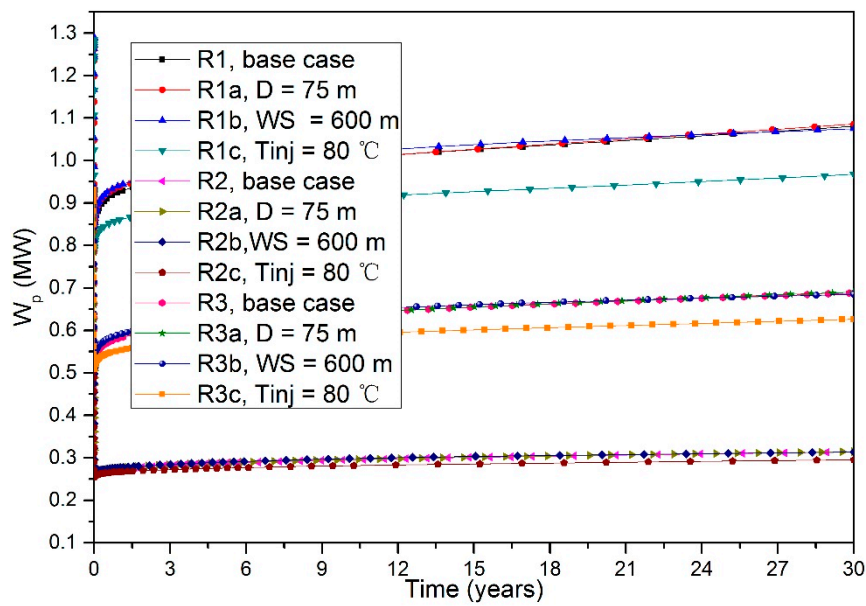**Figure 15.** Sensitivity of reservoir impedance to main parameters.

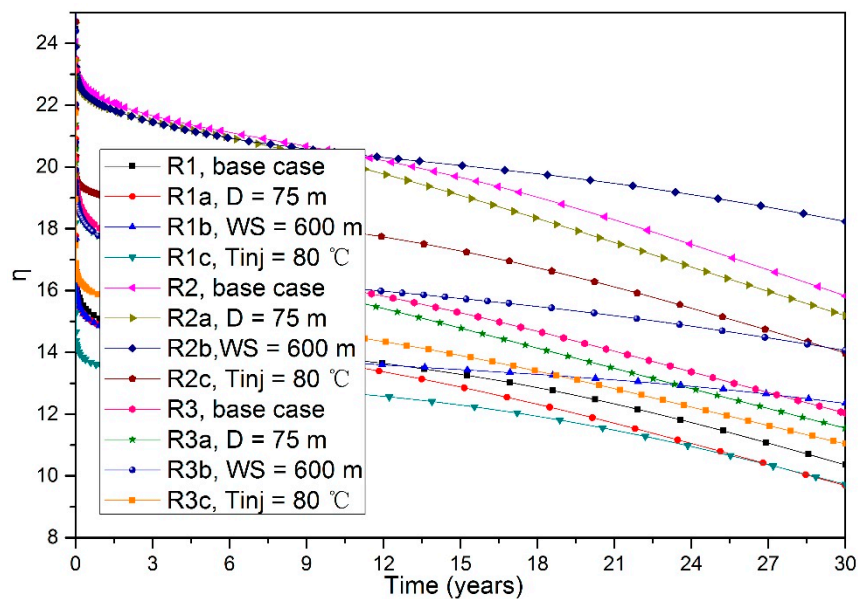**Figure 16.** Sensitivity of pump power to main parameters.

Figure 17. Sensitivity of energy efficiency to main parameters.

5.1. Sensitivity to Fracture Spacing

Figure 14 R1a shows that increasing D from 50 m to 75 m results in a decrease of W_e from 13.97–11.20 MW to 13.83–10.52 MW. For Figure 14 R2a and R3a, we can also find that an increase of D will cause the reduction of W_e. This is mainly because the fracture spacing determines the heat transfer area between the fractured rock and circulating water, higher fracture spacing will decrease the ratio between surface area and reservoir volume, finally decrease the heat transfer area, and this will significantly reduce the W_e according to the heat transfer formula. These are in agreement with studies from Sanyal et al. [22]. Figure 15 R1a shows that increasing D from 50 m to 75 m results in only very slight influence on the I_R. For Figure 15 R2a and Figure 15 R3a, similarly we can find that the increase of D has only very slight influence on the I_R. This is because the I_R is mainly determined by water viscosity and reservoir permeability [4,5]. In this study, the viscosity and reservoir permeability are all independent of the D, thus the change of the D has only a very slight effect on the I_R. This is in accordance with previous studies from Zeng et al. [33]. Figure 16 R1a shows that increasing D from 50 m to 75 m results in only a very slight influence on the W_p. For Figure 16 R2a and Figure 16 R3a, similarly we can find that the increase of D has only a very slight influence on the W_p. Because the increase of D has only a very slight influence on the I_R, based on Equations (12) and (16), the increase of D also has only a very slight effect on the P_{inj} and thus has only a slight effect on the W_p according to Equation (16). This is in accordance with previous studies by Zeng et al. [33]. Figure 17 R1a shows that increasing D from 50 m to 75 m results in a decrease of η from 20.62–10.36 to 19.31–9.69. For Figure 17 R2a and R3a, similarly we can find that the increase of D will cause the reduction of the η. This is because the increase of D will reduce the W_e, while only has a very slight influence on the W_p, based on Equation (17) this will obviously decrease the η. This is in accordance with previous studies from Zeng et al. [33]. Overall, the D has a significant influence on the electricity generation performance, within a certain range, increasing D will reduce the W_e, while have only a very slight effect on the I_R and W_p, thus significantly decrease the η.

5.2. Sensitivity to Well Spacing

Figure 14 R1b shows that increasing WS from 500 m to 600 m results in an increase of W_e from 13.97–11.20 MW to 19.72–13.27 MW. For Figure 14 R2b and R3b, similarly we can find that the increase of WS will cause the rise of W_e. This is because higher WS increases the reservoir volume between the injection well and production well, thus increases the T_{pro} and h_{pro}, according to Equation (11)

this obviously increases the W_e. This proves that the WS is an important design parameter for EGS construction, it is directly related to the W_e, thus the determination of WS should be based on an accurate analysis of the geological data of the geothermal field. Figure 15 R1b shows that increasing WS from 500 m to 600 m results in only a very slight influence on the I_R. For Figure 15 R2b and Figure 15 R3b, similarly we can find that the increase of WS has only a very slight effect on the I_R. As stated above, the I_R is mainly determined by water viscosity and reservoir permeability—the viscosity and permeability are independent of WS, thus it has only a very slight influence on the I_R. Figure 16 R1b shows that increasing WS from 500 m to 600 m results in only a very slight influence on the W_p. For Figure 16 R2b and R3b, similarly we can find that the increase of WS has only a very slight effect on the W_p. This is mainly because the increase of WS has only a very slight on the I_R, based on Equations (12) and (16), the increase of WS has only a very slight influence on the P_{inj} and W_p. Figure 17 R1b shows that increasing WS from 500 m to 600 m results in an increase of η from 20.62–10.36 to 22.56–12.35. For Figure 17 R2b and R3b, similarly we can find that an increase of WS significantly increases the η. As stated above, this is because the increase of WS obviously increases the W_e, while it has only a very slight effect on the W_p, based on Equation (17) this will increase the η. Overall, the WS has a significant influence on the electricity generation performance, within a certain range, increasing the WS will significantly increase the W_e, while have only a very slight effect on the I_R and W_p, thus significantly increase the η.

5.3. Sensitivity to Injection Temperature

Figure 14 R1c shows that increasing the T_{inj} from 60 °C to 80 °C results in a decrease of W_e from 13.97–11.20 M to 12.06–9.41 MW. For Figure 14 R2c and R3c, similarly we can find that the increase of the T_{inj} reduces the W_e. This is in accordance with previous studies from Zeng et al. [4,5]. This is because the increase of T_{inj} increases the h_{inj}, based on Equation (11) when the other conditions are unchanged, this will significantly decrease the W_e. Figure 15 R1c shows that increasing the T_{inj} from 60 °C to 80 °C results in a decrease of I_R from 0.097–0.128 MPa/(kg/s) to 0.095–0.115 MPa/(kg/s). For Figure 15 R2c and R3c, similarly we can find that the increase of the T_{inj} will significantly reduce the I_R. As mentioned above, the I_R is mainly determined by the water viscosity and reservoir permeability [4,5]. The increase of T_{inj} will increase the reservoir temperature, decrease the water viscosity, thus reducing the I_R. This is in accordance with previous studies by Zeng et al. [33]. Figure 16 R1c shows that increasing the T_{inj} from 60 °C to 80 °C results in a decrease of W_p from 0.82–1.08 MW to 0.80–0.97 MW. For Figure 16 R2c and R3c, similarly we can see that the increase of the T_{inj} will significantly decrease the W_p. This is because the increase of the T_{inj} reduces the I_R, according to Equations (12) and (16), this will significantly reduce the P_{inj} and thus further decrease the W_p. Figure 17 R1c shows that increasing the T_{inj} from 60 °C to 80 °C results in a decrease of the η from 20.62–10.36 to 18.20–9.73. For Figure 17 R2c and R3c, similarly we can find that the increase of the T_{inj} will significantly reduce the η. This is a comprehensive result of both reduction of W_e and W_p. Overall, the T_{inj} has a significant influence on the electricity generation performance, within a certain range, increasing the T_{inj} will reduce the W_e, decrease the I_R and W_p, and thus reduce the η.

6. Conclusions

In this study, we numerically investigated the influence of reservoir heterogeneity on the electricity generation performance of an EGS reservoir and analyzed the main factors affecting the production performance. The conclusions are as follows:

(1) With increasing of the reservoir heterogeneity, the water conduction ability of the reservoir gradually decreases, the available water production rate gradually reduces, thus the electric power gradually decreases.

(2) With increasing of the reservoir heterogeneity, the reservoir impedance gradually increases.

(3) With increasing of the reservoir heterogeneity, the pump power gradually reduces.

(4) With increasing of the reservoir heterogeneity, the energy efficiency gradually increases.

(5) The reservoir heterogeneity has a significant influence on the fracture temperature field. In higher permeability layers, a cold front will form and make the temperature distribution along depth uneven.

(6) The fracture spacing has a significant influence on the electricity generation performance, within a certain range, increasing the fracture spacing will obviously reduce the electric power, while having only very slight effect on the reservoir impedance and pump power, thus significantly decreasing the energy efficiency.

(7) The well spacing has a significant influence on the electricity generation performance, within a certain range, increasing the well spacing will obviously increase the electric power, while having only very slight effect on the reservoir impedance and pump power, thus significantly increasing the energy efficiency.

(8) The injection temperature has a significant influence on the electricity generation performance, within a certain range, increasing the injection temperature will obviously reduce the electric power, decrease the reservoir impedance and pump power, thus reducing the energy efficiency.

Conflicts of Interest: The authors declare no conflict of interest.

Nomenclature

D	fracture spacing, m
g	gravity, 9.80 m/s^2
h	well depth, m
h_1	depth of injection well, m
h_2	depth of production well, m
h_{inj}	injection specific enthalpy, kJ/kg
h_{pro}	production specific enthalpy, kJ/kg
I_R	reservoir impedance, MPa/(kg/s)
k	reservoir permeability, m^2
k_f	fracture permeability, m^2
k_m	matrix permeability, m^2
k_x	intrinsic permeability along x, m^2
k_y	intrinsic permeability along y, m^2
k_z	intrinsic permeability along z, m^2
P	pressure, MPa
P_{max}	critical pressure, MPa
P_{inj}	injection pressure, MPa
P_{pro}	production pressure, MPa
P_0	bottomhole production pressure, MPa
q	water production rate, kg/s
Q	total water production rate, kg/s
T	temperature, °C
T_0	mean heat rejection temperature, 282.15 K
T_{pro}	production temperature, °C
T_{inj}	injection temperature, °C
W_P	electric power of pump, MW
WS	well spacing, m
W_e	electric power, MW

x, y, z   cartesian coordinates, m
ϕ reservoir porosity
η energy efficiency
η_P pump efficiency, 80%
ρ water density, kg/m^3

References

1. Tester, J.W.; Livesay, B.; Anderson, B.J.; Moore, M.C.; Bathchelor, A.S.; Nichols, K.; Blackwell, D.D.; Petry, S.; Dipoppo, R.; Toksoz, M.N.; et al. *The Future of Geothermal Energy: Impact of Enhanced Geothermal Systems (EGS) on the United States in the 21st Century. An assessment by an MIT-Led Interdisciplinary Panel*; MIT: Cambridge, MA, USA, 2006.

2. Zhao, Y.S.; Wan, Z.J.; Kang, J.R. *Introduction to HDR Geothermal Development*; Science Press: Beijing, China, 2004. (In Chinese)

3. Wang, J.; Hu, S.; Pang, Z.; He, L.; Zhao, P.; Zhu, C.; Rao, S.; Tang, X.; Kong, Y.; Luo, L.; et al. Estimate of geothermal resources potential for hot dry rock in the continental area of China. *Sci. Technol. Rev.* **2012**, *30*, 25–31. (In Chinese)

4. Zeng, Y.C.; Tang, L.S.; Wu, N.Y.; Cao, Y.F. Analysis of influencing factors of production performance of enhanced geothermal system: A case study at Yangbajing geothermal field. *Energy* **2017**, *127*, 218–235. [CrossRef]

5. Zeng, Y.; Su, Z.; Wu, N. Numerical simulation of heat production potential from hot dry rock by water circulating through two horizontal wells at Desert Peak geothermal field. *Energy* **2013**, *56*, 92–107. [CrossRef]

6. Pruess, K. Modelling of geothermal reservoirs: Fundamental processes, computer simulation, and field applications. In Proceedings of the 10th New Zealand Geothermal Workshop, Auckland, New Zealand, 2–4 November 1988.

7. Willis-richards, J.; Wallroth, T. Approaches to the modeling of HDR reservoirs: A review. *Geothermics* **1995**, *24*, 307–332.

8. Hayashi, K.; Willis-Richards, J.; Hopkirk, R.J.; Niibori, Y. Numerical models of HDR geothermal reservoirs—A review of current thinking and progress. *Geothermics* **1999**, *28*, 507–518. [CrossRef]

9. Sanyal, S.K.; Butler, S.J.; Swenson, D.; Hardeman, B. Review of the state-of-the-art of numerical simulation of enhanced geothermal system. In Proceedings of the World Geothermal Congress, Kyushu-Tohoku, Japan, 28 May–10 June 2000.

10. O'Sullivan, M.J.; Pruess, K.; Lippmann, M.J. State of the art of geothermal reservoir simulation. *Geothermics* **2001**, *30*, 395–429. [CrossRef]

11. Birdsell, S.; Robinson, B. A three-dimensional model of fluid, heat, and tracer transport in the Fenton Hill hot dry rock reservoir. In Proceedings of the Thirteenth Workshop on Geothermal Reservoir Engineering, Stanford, CA, USA, 19–21 January 1988.

12. Mcdermott, C.I.; Randriamanjatosoa, A.R.; Tenzer, H.; Kolditz, O. Simulation of heat extraction from crystalline rocks: The influence of coupled processes on differential reservoir cooling. *Geothermics* **2006**, *35*, 321–344. [CrossRef]

13. Watanabe, N.; Wang, W.Q.; McDermott, C.I.; Taniguchi, T.; Kolditz, O. Uncertainly analysis of thermo-hydro-mechanical coupled processes in heterogeneous porous media. *Comput. Mech.* **2010**, *45*, 263–280.

14. Yuchao, Z.; Nengyou, W.; Zheng, S. Numerical simulation of heat production potential from hot dry rock by water circulating through a novel single vertical fracture at Desert Peak geothermal field. *Energy* **2013**, *63*, 268–282.

15. Yuchao, Z.; Nengyou, W.; Zheng, S. Numerical simulation of electricity generation potential from fractured granite reservoir through a single horizontal well at Yangbajing geothermal field. *Energy* **2014**, *65*, 472–487.

16. Yuchao, Z.; Jiemin, Z.; Nengyou, W. Numerical simulation of electricity generation potential from fractured granite reservoir through vertical wells at Yangbajing geothermal field. *Energy* **2016**, *103*, 290–304.

17. Yuchao, Z.; Jiemin, Z.; Nengyou, W. Numerical investigation of electricity generation potential from fractured granite reservoir by water circulating through three horizontal wells at Yangbajing geothermal field. *Appl. Therm. Eng.* **2016**, *104*, 1–15.

18. Yuchao, Z.; Jiemin, Z.; Nengyou, W. Numerical investigation of electricity generation potential from fractured granite reservoir through a single vertical well at Yangbajing geothermal field. *Energy* **2016**, *114*, 24–39.

19. Yuchao, Z.; Liansheng, T.; Nengyou, W.; Jing, S.; Yifei, C. Orthogonal test analysis on conditions affecting electricity generation performance of an enhanced geothermal system at Yangbajing geothermal field. *Energies* **2017**, *10*, 2015.

20. Cheng, W.L.; Wang, C.L.; Nian, Y.L.; Han, B.B.; Liu, J. Analysis of influencing factors of heat extraction from enhanced geothermal systems considering water losses. *Energy* **2016**, *115*, 274–288. [CrossRef]

21. Hu, L.T.; Winterfeld, P.H.; Fakcharoenphol, P.; Wu, Y.S. A novel fully-coupled flow and geomechanics model in enhanced geothermal reservoirs. *J. Petrol. Sci. Eng.* **2013**, *107*, 1–11. [CrossRef]

22. Sanyal, S.K.; Butler, S.J. An analysis of power generation prospects from enhanced geothermal systems. In Proceedings of the World Geothermal Congress 2005, Antalya, Turkey, 24–29 April 2005; pp. 1–6.

23. Taron, J.; Elsworth, D.; Min, K.B. Numerical simulation of thermal-hydrologic-mechanical-chemical processes in deformable, fractured porous media. *Int. J. Rock Mech. Min. Sci.* **2009**, *46*, 842–854. [CrossRef]

24. Taron, J.; Elsworth, D. Thermal-hydrologic-mechanical-chemical processes in the evolution of engineered geothermal reservoirs. *Int. J. Rock Mech. Min. Sci.* **2009**, *46*, 855–864. [CrossRef]

25. Gelet, R.; Loret, B.; Khalili, N. A thermal-hydro-mechanical coupled model in local thermal non-equilibrium for fractured HDR reservoir with double porosity. *J. Geophys. Res.* **2012**, *117*, 1–23. [CrossRef]

26. Gelet, R.; Loret, B.; Khalili, N. Thermal recovery from a fractured medium in local thermal non-equilibrium. *Int. J. Numer. Anal. Method Geomech.* **2013**, *37*, 2471–2501. [CrossRef]

27. Benato, S.; Taron, J. Desert Peak EGS: Mechanisms influencing permeability evolution investigated using dual-porosity simulator TFReact. *Geothermics* **2016**, *63*, 157–181. [CrossRef]

28. Pruess, K. Enhanced geothermal system (EGS) using CO_2 as working fluid-A novel approach for generating renewable energy with simultaneous sequestration of carbon. *Geothermics* **2006**, *35*, 351–367. [CrossRef]

29. Pruess, K. On production behavior of enhanced geothermal systems with CO_2 as working fluid. *Energy Convers. Manag.* **2008**, *49*, 1446–1454. [CrossRef]

30. Spycher, N.; Pruess, K. A phase-partitioning model for CO_2-brine mixtures at elevated temperatures and pressures: Application to CO_2-enhanced geothermal systems. *Transp. Porous Media* **2010**, *82*, 173–196. [CrossRef]

31. Borgia, A.; Pruess, K.; Kneafsey, T.J.; Oldenburg, C.M.; Pan, L. Numerical simulation of salt precipitation in the fractures of a CO_2-enhanced geothermal system. *Geothermics* **2012**, *44*, 13–22. [CrossRef]

32. Xu, T.F.; Yuan, Y.L.; Jia, X.F.; Lei, Y.D.; Li, S.T.; Feng, B.; Hou, Z.Y.; Jiang, Z.J. Prospects of power generation from an enhanced geothermal system by water circulation through two horizontal wells: A case study in the Gonghe Basin, Qinghai Province, China. *Energy* **2018**, *148*, 196–207. [CrossRef]

33. Zeng, Y.; Tang, L.; Wu, N.; Cao, Y. Numerical simulation of electricity generation potential from fractured granite reservoir using the MINC method at the Yangbajing geothermal field. *Geothermics* **2018**, *75*, 122–136. [CrossRef]

34. Baujard, C.; Bruel, D. Numerical study of the impact of fluid density on the pressure distribution and stimulated volume in the Soultz HDR reservoir. *Geothermics* **2006**, *35*, 607–621. [CrossRef]

35. Kolditz, O.; Clauser, C. Numerical simulation of flow and heat transfer in fractured crystalline rocks: Application to the hot dry rock site in Rosemanowes. *Geothermics* **1998**, *27*, 1–23. [CrossRef]

36. Kolditz, O. Modelling flow and heat transfer in fractured rocks: Conceptual model of a 3-D deterministic fracture network. *Geothermics* **1995**, *24*, 451–470. [CrossRef]

37. Jing, Z.; Willis-Richards, J.; Hashida K, W. A three-dimensional stochastic rock mechanics model of engineered geothermal systems in fractured crystalline rock. *J. Geophys. Res.* **2000**, *105*, 23663–23679. [CrossRef]

38. Jing, Z.; Watanabe, K.; Willis-Richards, J.; Hashida, T. A 3-D water/rock chemical interaction model for prediction of HDR/HWR geothermal reservoir performance. *Geothermics* **2002**, *31*, 1–28. [CrossRef]

39. Jing, Y.N.; Jing, Z.Z.; Willis-Richards, J.; Hashida, T. A simple 3-D thermoelastic model for assessment of the long-term performance of the Hijiori deep geothermal reservoir. *J. Volcanol. Geotherm. Res.* **2014**, *269*, 14–22. [CrossRef]

40. Sun, Z.X.; Zhang, X.; Xu, Y.; Yao, J.; Wang, H.X.; Lv, S.H.; Sun, Z.L.; Huang, Y.; Cai, M.Y.; Huang, X.X. Numerical simulation of the heat extraction in EGS with thermal-hydraulic-mechanical coupling method based on discrete fractures model. *Energy* **2017**, *120*, 20–33. [CrossRef]

41. Yao, J.; Zhang, X.; Sun, Z.X.; Huang, Z.Q.; Liu, J.R.; Li, Y.; Xin, Y.; Yan, X.; Liu, W.Z. Numerical simulation of the heat extraction in 3D-EGS with thermal-hydraulic-mechanical coupling method based on discrete fractures model. *Geothermics* **2018**, *74*, 19–34. [CrossRef]

42. Huang, W.; Cao, W.; Jiang, F. Heat extraction performance of EGS with heterogeneous reservoir: A numerical evaluation. *Int. J. Heat Mass Transfer* **2017**, *108*, 645–657. [CrossRef]

43. Zarrouk, S.J.; Moon, H. Efficiency of geothermal power plants: A worldwide review. *Geothermics* **2014**, *51*, 142–153. [CrossRef]

44. Pruess, K.; Oldenburg, C.; Moridis, G. *TOUGH2 User's Guide, Version 2.0*; Lawrence Berkeley National Laboratory: Berkeley, CA, USA, 1999.

45. Asai, P.; Panja, P.; Mclennan, J.; Moore, J. Performance evaluation of enhanced geothermal system (EGS): Surrogate models, sensitivity study and ranking key parameters. *Renew. Energy* **2018**, *122*, 184–195. [CrossRef]